Improved photophysical properties of ionic materialbased combination chemo/PDT nanomedicine

Samantha Macchi^a, Mohd Zubair^b, Robert Hill^a, Nabeel Alwan^a, Yusuf Khan^c, Nawab Ali^b, Grégory Guisbiers^d, Brian Berry^a, and Noureen Siraj^{a,*}

- [a] Department of Chemistry. University of Arkansas at Little Rock. 2801 S. University Ave., Little Rock, AR 72204, USA
- [b] Department of Biology. University of Arkansas at Little Rock. 2801 S. University Ave., Little Rock, AR 72204, USA
- [c] Department of Electrical and Computer Engineering, University of Texas at Austin, Austin, TX 78712, USA
- [d] Department of Physics and Astronomy. University of Arkansas at Little Rock.2801 S. University Ave., Little Rock, AR 72204, USA

Keywords: ionic liquids, cytotoxicity, ionic materials, photodynamic therapy, porphyrin

Abstract

Herein, a cost effective and prompt approach to develop ionic material-based combination nanodrugs for cancer therapy is presented. A chemotherapeutic (phosphonium) cation and photodynamic therapeutic (porphyrin) anion are combined using a single step ion exchange reaction. Afterwards, a nanomedicine is prepared form these ionic materials-based combination drug using a simplistic strategy of reprecipitation. Improved photophysical characteristics such as slower non-radiative rate constant, enhanced phosphorescence emission, longer lifetime, and bathochromic shift in absorbance spectra of porphyrin is observed in the presence of a chemotherapeutic counter cation. The photodynamic therapeutic activity of nanomedicines is investigated by measuring the singlet oxygen quantum yield using two probes. Compared to parent porphyrin compound, the synthesized combination material showed a two-fold increase in the reactive oxygen species quantum yield, due to inhibition of face-to-face aggregation of porphyrin units in the presence of bulky chemotherapeutic ions. The dark cytotoxicity of combination therapy nanomedicines in MCF-7 (cancerous breast) cell line is also increased as compared to their corresponding parent compounds in vitro. This is due to high cellular uptake of the combination nanomedicines as compared to free drug. Further, selective toxicity towards cancer cells was acquired by functionalizing nanomedicine with folic acid followed by incubation with MCF-7 and MCF-10A (non-cancerous breast). Light toxicity experiments indicate that the synthesized ionic nanomedicine shows greater cell death than either parent drug due to improved photophysical properties and effective combination effect. This facile and economical strategy can easily be

utilized in the future to develop many other combination ionic nanomedicines with improved photodynamics.

1. Introduction

Cancer is currently the second leading cause of death in the world, only behind heart disease. In the US, the death toll is projected to be 606,520 people (2020), making up nearly twenty two percent of overall deaths. Commonly utilized therapies such as chemotherapy, radiation, and surgery, are highly invasive with extreme side effects for the patient. Therefore, the development of new cancer therapy practices is of utmost importance. One promising method to treat cancer is the use of combination therapy. In combination therapy, two or more therapeutic mechanisms are combined in a single drug to improve the anticancer effects compared to one method alone. Furthermore, this approach potentially minimizes harmful side effects and combats drug resistance by using a lower dose of each drug/treatment.² There are numerous potential combinations of drugs and treatments, but one that has gained particular interest in recent years is the tandem use of chemotherapy and photodynamic therapy (PDT).^{3,4} For effective treatment of advanced cancer, the Food and Drug Administration (FDA) has approved several combinations of medication. ^{5,6} However, currently available combination drugs are costly due to their complicated synthesis protocol. 7-9 Therefore, it is imperative to develop new economical drugs using a simple, rapid, and inexpensive approach with advanced properties. In this study, a new class of compounds is introduced i.e., ionic materials (IMs) to develop a combination therapy medicine.

IMs, sometimes called frozen ionic salts, are a subclass of ionic liquids (ILs) and share many of the same characteristics, except that they are solids at room temperature. The main reason for their low melting point is the presence of bulky, long chain, often organic ions which makes the packing of ions less efficient due to steric hindrance. These materials are highly

thermally stable and tunable in their chemical and photophysical properties. Therefore, they have been explored for multiple applications. ^{11–17} ILs are highly tunable where both counterions can be easily exchanged to fit specific applications. The cationic nitrogen and phosphorus based ILs, have gained attention in regards to their chemotherapeutic activity. ^{18–21} Some of the ILs show cytotoxicity towards normal cells which has restricted their use for medical applications. In this project, for the first time, a chemo-PDT combination nanomedicine from IMs was developed.

Many recent advances in cancer research seek to address the undesirable toxicity of chemotherapeutic agents towards normal cells. It is evident that nanomaterials have shown greater potential in cancer research for several reasons, including greater cellular uptake and enhanced permeability and retention (EPR) phenomenon. This has led to the use of nanoparticles (NPs) due to their increased intracellular concentration in cancer cells and lower toxicity in normal cells. Many inorganic NPs including heavy metals, metal oxides, and quantum dots have been developed for cancer therapy. These toxic, non-biodegradable inorganic NPs may cause detrimental effects on normal cells. Therefore, organic NPs are currently attracting considerable attention among researchers due to their excellent biocompatibility, biodegradability and non-toxicity. The his regard, IMs are highly applicable in the field of cancer research due to their ability to form ionic nanomaterials (INMs) where room temperature ILs can form nanodroplets which are not true NPs and are often unstable. In this study, carrier free INMs without the use of any matrix are presented for the first time as combination therapy nanomedicines for cancer.

Cancer nanodrugs are also commonly surface functionalized with targeting agents to enhance the selective toxicity of the drugs towards cancer cells. This technique can also alter the cellular uptake mechanism by adding receptor mediated uptake routes. Some promising molecules used for coating drugs include polymers, specific antibodies, and small molecules etc. ^{35,36} Folic acid (FA) is a common small molecule targeting agent as it has been shown that folate receptors are overexpressed in certain types of solid tumors in breast, lung, and epithelial tissues. ³⁷ Mostly, folic acid moieties are covalently attached to drugs to enhance selective toxicity towards cancer cells. ³⁸ However, this is a complex, time consuming, costly and low yield methodology. Therefore, it is of utmost importance to seek a simple and cost-effective strategy to functionalize the surface of NPs. In the present study, porphyrin-based combination nanomedicine's surface is coated with folate using ionic and intermolecular interactions.

An effective photosensitizer (PS) is of critical importance for effective PDT. An ideal PS possesses several characteristics such as absorption wavelength maxima at longer wavelength to treat deeper seated tumors in the body, high singlet oxygen quantum yield, high molar absorptivity, and no dark toxicity. Porphyrin molecules are very well studied in terms of their application in PDT.^{29,39,40} Previous work using porphyrin based INMs showed enhanced photophysical properties as PDT PSs.^{41,42} Several studies have been performed to improve the PDT efficiency of porphyrin by inhibiting aggregation in the planer structure of porphyrin.^{30,40,42} A simplistic approach to improve photophysical properties is acquired by replacing the small counterion of porphyrin with a bulky moiety to prevent face aggregation that would otherwise reduce PDT efficiency of the drug.

In this study, a chemotherapeutic phosphonium cation, trihexyltetradecylphoshonium (P_{66614}^+) is paired with a photosensitizing anion, meso-tetra(4-carboxyphenyl)porphyrin (TCPP⁴⁻) to produce a single molecule IM, tetra(trihexyltetradecylphosphonium) meso tetrakis(4-carboxyphenyl)porphyrin ([P₆₆₆₁₄]₄[TCPP]) combination drug. This chemotherapeutic and photodynamic therapeutic (chemo-PDT) IM is a hydrophobic compound which can easily be

converted to INMs in aqueous/buffer solution via reprecipitation. 41,42 These INMs are highly tunable, and their surface charge is altered by functionalization with folate to enhance cellular uptake and selective cytotoxicity towards cancerous cells. INMs' surface charge and hydrodynamic radius are also determined. The photophysical properties of parent porphyrin compound (porphyrin), IMs ([P₆₆₆₁₄]₄[TCPP]) and its INMs are studied in detail to investigate their potential as PDT nanodrug. The singlet oxygen quantum yield is also investigated using a probe to determine the PDT activity of IMs. The cytotoxicity of the carrier-free nanodrugs, before and after functionalization with folate, is investigated *in vitro* using two cell lines (cancerous and noncancerous cells). To the best of our knowledge, this is the first report where ILs chemistry approach has been used to develop combination therapeutic nanomedicines for cancer therapy application.

2. Materials and Methods

2.1. Chemicals. Trihexyltetradecylphosphonium chloride ($P_{66614}Cl$) was purchased from Sigma Aldrich (St. Louis, MO) and porphyrin (TCPP) was purchased from Tokyo Chemical Industry (Tokyo, Japan). FA was purchased from Calbiochem (San Diego, CA). 1,3-diphenylisobenzofuran (DPBF) and 9,10-anthracenediyl-bis(methylene)dimalonic acid (ABDA) were purchased from Sigma Aldrich. Sodium hydroxide and methylene blue (MB) were purchased from VWR (Radnor, PA). All chemicals were used as received and only TCPP was modified prior to IMs synthesis. Triply deionized water (18.2 M Ω cm) was obtained using Purelab Ultrapure water purification system (ELGA, Woodridge, IL). Dichloromethane (DCM) and ethanol were of ACS grade and purchased from Thermo Fisher (Waltham, MA). MTT (3-(4,5-dimethylthiazol-2-yl)-2,5-diphenyltetrazolium bromide) and PBS buffer (pH 7.4) and dimethylsulfoxide (DMSO) were purchased from Sigma Aldrich. DMSO was filtered through a 0.2 micron polytetrafluoroethylene (PTFE) filter prior to use.

2.2. Synthesis and characterization of IMs for combination cancer therapy. The combination therapy drug was synthesized from two parent compounds utilizing a simple, rapid, economical one-step ion exchange method. P₆₆₆₁₄Cl, was used as the chemotherapeutic compound and TCPP acted as the PDT drug (Figure 1). Solution A was prepared by dissolving P₆₆₆₁₄Cl in DCM. Solution B was prepared by deprotonation of TCPP with 6 molar equivalents of sodium hydroxide in water. This mixture was allowed to stir for 30 minutes to ensure full deprotonation of all four carboxylic protons. Aqueous Solution B of 1 mol equivalent sodium salt of TCPP (Na₄TCPP), was then added to a reaction vessel containing 4 mol equivalent of Solution A (in DCM) in 1:2 v/v ratio. The reaction vessel was stirred for 24 hr to ensure complete ion exchange. Later, the water layer containing sodium chloride salt was discarded and the organic layer was washed three times with water to remove any remaining salt. The organic solvent layer was then dried via rotary evaporation to remove the DCM, and the resultant drug, [P₆₆₆₁₄]₄[TCPP] was collected, freeze dried to remove moisture, and used for further studies. The combination drug was characterized using Electrospray ionization mass spectrometry (ESI-MS) which was performed using a Bruker (Billerica, MA) Ultraflex 9.4T in methanol solvent. The mass-to-charge ratio peaks in positive and negative ion mode verified the presence of both the cation and anion in [P₆₆₆₁₄]₄[TCPP] (Figure S1 and S2 in the Supporting Information). Nuclear magnetic resonance (NMR, JEOL) was used to verify purity of [P_{66614}]₄[TCPP]. ¹H NMR (400 MHz, (CD₃)₂SO): δ -2.88 (s, 2H), 0.84 (m, 48H), 1.27 (q, 192H), 2.15 (t, 32H), 8.08 (d, 8H), 8.25 (d, 8H), 8.84 (s, 8H). NMR spectra is given in Figure S3 in the Supporting Information.

Figure 1. Scheme of IMs combination drug synthesis

2.3. Synthesis and characterization of INMs for combination cancer therapy. INMs were prepared by reprecipitation in water or cell media from IMs' stock solution in ethanol for spectroscopic measurements and in DMSO for cellular studies, respectively. Briefly, a stock solution of the combination drug was prepared at 1 mM concentration in ethanol or DMSO and was dropwise added to a scintillation vial of deionized water/cell media already present in an active sonication bath. The vial was allowed to sonicate for fifteen minutes with a thirty-minute rest period prior to measurements. For FA-functionalized INMs, stock solution of chemo-PDT IM in DMSO was added dropwise to a 100 µM solution of FA under sonication in the same manner as mentioned earlier for INM synthesis. FA-INMs were recovered by centrifugation. A NanoBrook 90PLUS (Brookhaven instruments corporation, Holtsville, NY) was used to determine the zeta potential and hydrodynamic diameter of INMs in DI water using dynamic light scattering method (DLS). Transmission electron microscopy (TEM) imaging was performed to characterize INMs size using JEOL FEI Tecnai F20 200 keV microscope. [P₆₆₆₁₄]₄[TCPP] INMs were prepared for TEM analysis by dropwise addition of 0.1 mL IM stock solution in 0.9 mL water under sonication followed by 30 min rest and subsequent centrifugation to concentrate particles. INMs were resuspended in water then 4 µL were drop-casted onto grids. Lacey carbon grids (Ted Pella, Redding, CA) were used for TEM imaging.

2.4. Photophysical properties. The absorption and fluorescence emission spectra of the parent compounds, the synthesized IMs, and INMs for combination cancer therapy were recorded and analyzed. UV-Visible spectrometer (Agilent Cary 5000, Santa Clara, CA) and fluorometer (Horiba Fluorolog, Kyoto, Japan) were used to record absorption and emission spectra respectively. Starna quartz cuvettes with 4 sides and 1 cm path length were used for fluorescence/phosphorescence emission measurements. Quantum yield measurements were performed using a relative method with TCPP as a standard in ethanol. The quantum yield of the IMs and INMs were determined, in ethanol solvent using the following Equation 1.

$$\Phi_{un} = \Phi_{s} \times \frac{l_{un}}{l_{s}} \times \frac{Abs_{s}}{Abs_{un}} \times \left(\frac{n_{un}}{n_{s}}\right)^{2} \tag{1}$$

where Φ_s is the quantum yield of the standard, I is the integrated fluorescence emission intensity, Abs is the absorbance at the excitation wavelength, and n is the refractive index of the standard (n_s) and unknown (n_{un}). Radiative and non-radiative rate constants were also calculated from photophysical data. From the absorbance and emission spectra, the radiative rate constant was calculated (k_{rad}) using the Stricker-Berg relationship (Equation 2).

$$k_{rad} = 2.88 \times 10^{-9} \times n^2 \times \frac{\int I(\tilde{v})d\tilde{v}}{\int I(\tilde{v})\tilde{v}^{-3}d\tilde{v}} \int \frac{\varepsilon(\tilde{v})}{\tilde{v}} d\tilde{v}$$
 (2)

where I is the emission intensity, ν is the wavenumber of light, and ϵ is the molar extinction coefficient. The radiative rate constant was used to determine the non-radiative rate constant (k_{non-rad}) from Equation 3.

$$\Phi_F = \frac{k_{rad}}{k_{rad} + k_{non-rad}} \tag{3}$$

Fluorescence lifetimes were recorded using time correlated single photon counting (TCSPC) method with DeltaHub controller in conjunction with Horiba fluorometer. NanoLED (Horiba) source (1 MHz, 390 nm excitation wavelength) was used as an excitation source. Data was processed with DAS6 software using exponential fitting of raw data. Phosphorescence emission was recorded using 0.1 ms delay time at low temperature (77 K). Phosphorescence decay was performed using Decay by Delay method and fit using one exponential.

2.5. Reactive oxygen species and singlet oxygen generation measurements. The reactive oxygen species (ROS) quantum yield of the parent TCPP and [P₆₆₆₁₄]₄[TCPP] chemo-PDT combination IMs was investigated to determine the efficiency of the PDT drug. The obtained results for parent and IMs were compared to investigate the changes in PDT performance of porphyrin drug when converted into combination cancer therapy IMs. DPBF was used as a ROS probe and ABDA was used as a singlet oxygen selective probe. DPBF is yellow in ethanol solution with absorption maximum wavelength at 411 nm. The probe is oxidized by singlet oxygen and other ROS, which disrupts its conjugated system and converts it into a transparent solution (cannot absorb light).⁴² Similarly, ABDA probe exhibits a decrease in absorbance at a wavelength maximum of 380 nm when reacted with singlet oxygen in water. In a typical experiment with DPBF, TCPP and the IM derived from TCPP were dissolved in ethanol, separately. Then, DPBF was dissolved in the same solvent and added to each drug solution separately with a final concentration of 5 µM drug in 100 µM DPBF. The rate of ROS produced was quantified by irradiating the solution at the wavelength maxima of TCPP and IMs (417 nm) for 60 s time intervals and a total irradiation time of 420 s using a fluorescence spectrofluorometer (14 nm slit) and then measuring the absorption spectra of the solution using UV visible spectrophotometer. The ROS produced during irradiation of TCPP/IMs was scavenged by DPBF. After each

irradiation treatment, changes in the absorbance intensity of DPBF at 411 nm were monitored using UV/Vis spectrophotometer. MB was used as a standard to calculate the ROS quantum yield of TCPP parent compound and IMs.

Using ABDA probe, because it is not as sensitive as DBPF, the final concentration of drug (TCPP or INMs) used was 10 μ M and probe concentration was 200 μ M in water. A similar irradiation protocol was followed as before, with slight modification. The solution was irradiated at 150 s intervals for a total time of 1200 s and absorbance decrease of ABDA was monitored at 380 nm upon reaction with singlet oxygen. ROS and singlet oxygen quantum yield were calculated using the following Equation 4.43

$$\Phi_{\Delta(x)} = \Phi_{\Delta(std)} \times \frac{S_x}{S_{std}} \times \frac{1 - 10^{-A_{std}}}{1 - 10^{-A_x}} \tag{4}$$

where S is the slope of the plot of probe absorbance versus time, A is the absorbance of sample without probe, and subscript x is the unknown sample (TCPP or $[P_{66614}]_4[TCPP]$) and subscript MB is the standard.⁴²

The absorption maxima wavelength of probes (DPBF/ABDA) and porphyrin are very close to each other. Thus, to prove that decrease in absorption intensity is due to probe reaction with ROS and not due to photobleaching of TCPP/IMs, another experiment was designed. In this experiment, only TCPP/IMs/INMs solution without any singlet oxygen probe was irradiated using a fluorometer. A second control experiment was designed in order to ensure photobleaching of the probe was due to singlet oxygen produced by the standard or porphyrin alone. In this experiment, only probe was irradiated under same parameters of the previous experiment.

2.6. Cell Culture/Cell Viability. Model human cell lines, MCF-7 cancerous and MCF-10A non-cancerous cells were purchased from American Type Culture Collection (ATCC, Manassas, VA). Dulbecco's modified Eagle's medium (DMEM), Trypsin-EDTA (0.25%), penicillin, streptomycin and minimal essential medium were purchased from Caisson Lab (Smithfield, UT). Fetal bovine serum (FBS) was obtained from Atlanta Biologicals (Lawrenceville, GA). Mammary epithelial cell basal medium, epidermal growth factor, insulin, hydrocortisone, bovine pituitary extract, gentamicin, and amphotericin B were all purchased from PromoCell (Heidelberg, DE). In vitro studies were performed using two cell lines, MCF-7 and MCF-10A. All cells were maintained in monolayer at 37 °C and 5% CO₂ in complete medium. MCF-7 cells were cultured in DMEM with phenol red, supplemented with FBS (10% v/v) and penicillin/streptomycin antibiotic solution (500 units/ml). MCF-10A cells were grown in mammary epithelial cell basal medium supplemented with epidermal growth factor (10 ng/mL), insulin (5 µg/mL), hydrocortisone (0.5 µg/mL), bovine pituitary extract (0.004 mL/mL), gentamicin (100 µg/mL), and amphotericin B (0.05 µg/mL). At desired confluence, cells were subcultured by trypsinization and detached cells were counted using a hemocytometer following staining with trypan blue exclusion dye.

In order to determine 24 hr dark toxicity, cells were seeded in 96 well plates at 10⁴ cells per well and incubated at 37 °C (5% CO₂) for 24 hrs. Cells were then treated with different concentrations of drug for 24 hr. INMs were prepared at various concentrations by diluting stock solution in cell culture media following bath sonication, while maintaining a sterile environment. DMSO used as a vehicle was at a maximum of 0.5% to avoid any cellular toxicity. Cells were treated with different concentration of drugs and incubated for 24 hr. Appropriate controls with complete media alone and vehicle control without drug (DMSO) were included. Following

treatment, cells were washed with PBS buffer. MTT assay was used to determine cell viability as described previously.⁴⁴ A microplate reader (Biotek Synergy H1, Winooski, VT) was used to determine optical density at 570 nm for MTT assay. For *in vitro* studies, each experiment was performed in triplicate and repeated three times. All data that show error bars are presented as mean ± standard deviation (SD) unless otherwise mentioned. The significance of difference in the mean values was determined using two-tailed student 't' test. Values with significant difference are denoted as * p<0.05, ** p<0.01, *** p<0.005.

Light toxicity experiments were performed in order to determine combination chemo-PDT effect intracellularly. Cells were treated in a similar manner as described above. Briefly, 10⁴ cells were plated in 96 well plate and allowed to incubate 24 hr. Afterwards, cells were treated with INMs or TCPP and incubated again for 4 hr. Then the media containing drug was removed and cells were washed thrice with PBS to remove external drug. Cell media was replaced in each well and the plate was irradiated with visible lamp (0.14 W/cm²) for 10 min. A control experiment was run in tandem with identical conditions but was not exposed to light. Following irradiation, the plate was incubated an additional 24 hr and MTT assay was used to determine cell viability.

Cellular uptake experiments were performed to investigate the amount of TCPP or INMs taken up by MCF-7 cells at a given time interval. 3.0×10^5 cells were seeded in 6 well plate and incubated at 37 °C for 24 hr. TCPP or INMs were added to each well at a final concentration of 2 μ M (in 2 mL) and incubated in the dark for 4 hr. After the allotted time, the cells were washed thoroughly with PBS three times to remove any external drug. Cells were dissolved with 3 mL DMSO and concentrations were determined by UV-Vis spectrophotometer.

3. Results and Discussion

3.1. Drug Characterization. Reprecipitation of combination cancer therapy IMs in water yielded spherical NPs which are reported by TEM to be 24.2±5.1 nm in diameter (Figure S4 in the Supporting Information). Solvated diameter of particles was analyzed using DLS method in water and was found to be 45.2±6.7 nm (Figure S5 in the Supporting Information). This value is approximately double the value obtained for dry NPs due to biasing of DLS measurements by inherent weighting factors.⁴² Upon coating with FA, the hydrodynamic diameter was further increased to 53.3±12.5 nm which proved the functionalization of INMs.

Zeta potential measurements were also performed for the NPs in water. The value of zeta potential for combination INMs were determined to be +33.5±4.7 mV. This high positive zeta potential indicates the presence of majority bulky phosphonium cations at the surface of INMs. The magnitude of the surface charge indicates a stable colloidal suspension of INMs in aqueous media. The positive surface charge of combination therapy nanomedicine may allow for enhanced preferential uptake by cells since the cellular membranes are negatively charged. Coating with FA yielded particles with zeta potential value of +17.2±2.5 mV. This indicates that negatively charged FA altered the surface charge of INMs combination drug, which further confirms the presence of folate ions at the surface of INMs.

3.2. Photophysical Characterization. Absorbance spectra of parent compound, TCPP, IM ([P₆₆₆₁₄]₄[TCPP]), and [P₆₆₆₁₄]₄[TCPP] INMs were recorded and compared. All compounds show characteristic spectra of porphyrins that contain a Soret band at ~415-420 nm and four Q-bands at approximately 515, 550, 590, and 650 nm (Figure 2a). Ethanolic solution of TCPP and [P₆₆₆₁₄]₄[TCPP] IMs shows similar wavelength maxima. However, a notable red shift in absorption

maxima wavelength is observed for aqueous $[P_{66614}]_4$ [TCPP] INMs as compared to TCPP in water. The Soret band position of [P₆₆₆₁₄]₄[TCPP] INMs in water is slightly red shifted from 415 to 420 nm compared to the parent dye, free TCPP in water. The largest bathochromic shift in wavelength is observed at the longest wavelength Q band from 638 to 652 nm. The shift of absorption maxima wavelength is highly desirable to attain better penetration depth of light in bodily tissue. These results indicate that improved photophysical properties of porphyrin are attained by attaching a bulky chemotherapeutic cation in IMs and INMs. A slight decrease in molar extinction coefficient at the Soret band wavelength is observed for [P₆₆₆₁₄]₄[TCPP] INMs in water than its parent dye in water (Table 1). This is attributed to the particle formation of combination therapy nanomedicines as compared to the soluble TCPP parent dye. In chemo-PDT INMs, porphyrin molecules are mostly present inside, and surface is covered with alkyl phosphonium ion (confirmed by positive zeta potential) which does not absorb light. Moreover, those porphyrin anions who reside at outer layer that can absorb light while the interaction of inner molecule of porphyrin in NPs with electromagnetic radiation can be weak. The difference in molar extinction values at the Q bands for TCPP and [P₆₆₆₁₄]₄[TCPP] compounds is much less than for the Soret bands. It is observed that the photophysical properties of a PDT drug are tuned by attaching four alkyl phosphonium chemotherapeutic cations. Thus, it is proved that ILs chemistry can be utilized to successfully tailor the photophysical properties of the PS used as PDT agent in combination cancer therapy. It is well known that planar porphyrins like TCPP may aggregate at elevated concentrations. 45,46 Thus, aggregation experiments were conducted for aqueous TCPP and [P₆₆₆₁₄]₄[TCPP] INMs at concentrations up to 0.05 mM. It was found that TCPP shows an additional peak at approximately 440 nm at high concentrations, (Figure S6 in the Supporting Information) indicating potential aggregation state. 47,48 No additional peak for INMs is seen at 0.05 mM, indicating that the

introduction of bulky phosphonium counterion effectively inhibits aggregation of TCPP units even at high concentration.

Upon coating the surface of INMs with FA, the functionalized INMs absorption spectrum remains similar in shape. The absorption peak maximum at 420 nm for [P₆₆₆₁₄]₄[TCPP] INMs spectrum is slightly red shifted to 425 nm when functionalized with FA (Figure S7 in the Supporting Information). There is also significant broadening of the Soret band in FA-coated INMs spectrum. As mentioned earlier, the longer wavelength absorption maxima are achieved in INMs when functionalized with FA, which is advantageous for PDT application because these nanomedicines can be used to treat deeply seated tumor due to the ability of longer wavelength light to penetrate deeper into the body tissue.

Fluorescence measurements for porphyrin-based compounds shows that [P₆₆₆₁₄]₄[TCPP] INMs fluorescence emission intensity is reduced and red shifted compared to free TCPP in water (Figure 2b). A similar trend is observed in the absorption spectra of the aforementioned samples. Therefore, fluorescence quantum yield and rate of decay (radiative and non-radiative) were investigated to predict the PS's performance in both compounds which is directly corelated the PDT efficiency.

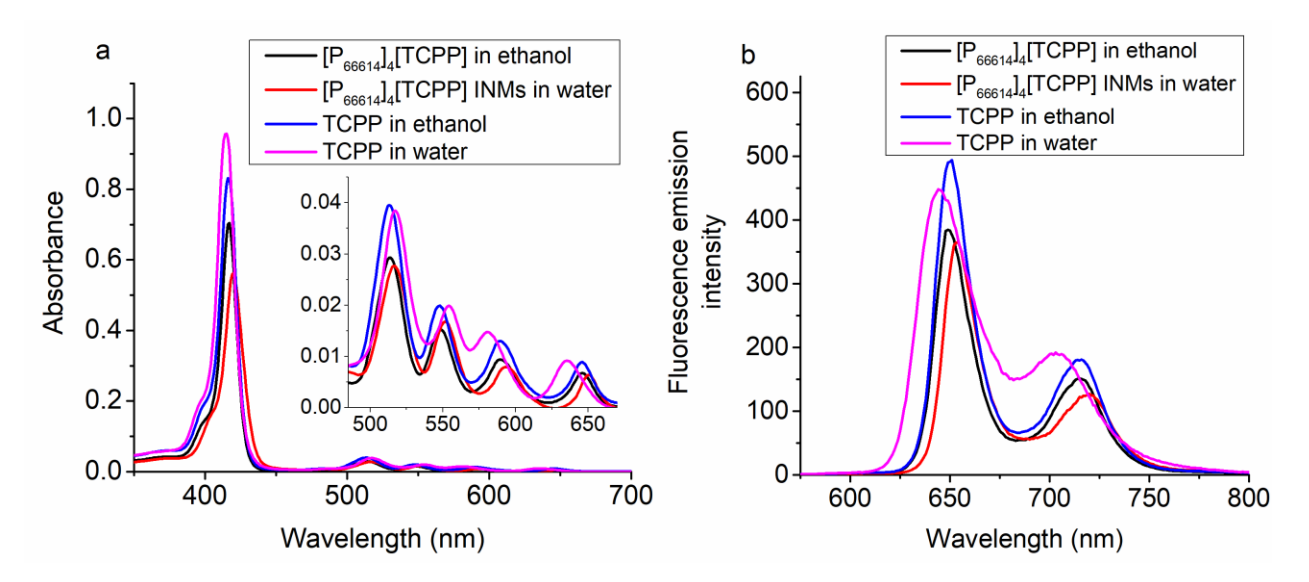


Figure 2. a) Absorption spectra and b) fluorescence emission spectra of 2.5 μM dye samples/INMs in water and in ethanol at an excitation wavelength of wavelength maximum for each sample at approximately 420 nm.

Table 1. Molar absorptivity of compounds in water and ethanol solvents

Compound	λ_{max} (nm)	ε (L·mol ⁻¹ cm ⁻¹)
TCPP in water	415, 517, 555, 580, 635	1.40×10^5 , 5.52×10^3 , 2.81×10^3 , 2.09×10^3 , 1.28×10^3
[P ₆₆₆₁₄] ₄ [TCPP] INMs in water	420, 516, 552, 593, 649	9.10×10^4 , 3.98×10^3 , 2.35×10^3 , 1.12×10^3 , 0.90×10^3
TCPP in ethanol	417, 514, 548, 588, 645	$1.21 \times 10^5, 5.69 \times 10^3, 2.83 \times 10^3, 1.77 \times 10^3, 1.22 \times 10^3$
[P ₆₆₆₁₄] ₄ [TCPP] in ethanol	417, 513, 548, 588, 645	$1.02 \times 10^5, 4.11 \times 10^3, 2.13 \times 10^3,$ $1.31 \times 10^3, 0.85 \times 10^3$

3.3. Quantum yield and photophysical rate constants. Fluorescence quantum yield measurements were performed to investigate the change in quantum yield upon conversion of porphyrin into IMs and INMs. In this experiment, TCPP was used as a standard compound as it

shows absorption in a similar wavelength region. The quantum yield of the IMs and INMs were determined in ethanol solvent using Equation 1. TCPP has a literature quantum yield value of 0.044 in ethanol which is used as a standard here.⁴⁹ After deprotonation in water, the quantum yield is enhanced up to 0.058 (Table 2). This could be due to polarity induced structural changes, commonly seen in fluorophores,⁵⁰ such as lowered aggregation of the porphyrin unit in water as compared to ethanol. Aggregation can quench fluorescence and thus lead to lower quantum yields. Upon conversion of TCPP to IM, [P₆₆₆₁₄]₄[TCPP], quantum yield is slightly higher than its parent compound with a value of 0.048 in ethanol solvent. This increase in quantum yield value is attributed to the presence of bulky phosphonium moieties which minimized the aggregations of porphyrin moieties in ethanol. However, INMs exhibited lower fluorescence quantum yield as compared to the parent porphyrin compound, which indicates the chances of an improved intersystem crossing process that is essential to develop effective PDT nanomedicine. FA-INMs showed even lower quantum yield of 0.016, which is indicative of other possible transitions.

The radiative and non-radiative rates were also investigated (using Equation 2 and 3) as these parameters can shed light on PDT mechanism of the PSs. It is noteworthy that IM and INMs show slower radiative and non-radiative decay rates as compared to parent compound (Table 2). Additionally, FA-INMs show a similar radiative rate constant compared to INMs. Results of photophysical characterization suggest that there is a possibility of increased triplet state population in INMs which can consequently enhance the PDT efficiency of INMs by converting molecular oxygen into singlet oxygen in the excited triplet state. Therefore, phosphorescence emission experiments are performed.

Table 2. Fluorescence quantum yield and radiative/non radiative rates of PSs

Compound	Φ_{F}	$k_{rad}/s^{\text{-}1} \times 10^6$	$k_{non-rad}/s^{-1} \times 10^7$
TCPP in water	0.058	1.09	2.39
[P ₆₆₆₁₄] ₄ [TCPP] INMs in water	0.050	0.79	1.50
FA functionalized [P ₆₆₆₁₄] ₄ [TCPP] INMs in water	0.016	0.80	5.04
TCPP in ethanol	0.044^{1}	1.10	1.78
[P ₆₆₆₁₄] ₄ [TCPP] in ethanol	0.048	0.80	1.57

¹This value was obtained from Reference [39]

3.4. Phosphorescence emission spectra. The existence of a triplet excited state is a crucial requirement for a PDT drug to generate singlet oxygen species. The photodynamics of the triplet state can shed light on the PDT capability of a PS. Phosphorescence of TCPP and [P₆₆₆₁₄]₄[TCPP] were recorded separately in ethanol at 77 K. It was found that [P₆₆₆₁₄]₄[TCPP] shows much more intense phosphorescence emission compared to its parent porphyrin at the same concentration (Figure S8 in the Supporting Information). This further confirms the greater populated first excited triplet state (T₁) of IM compared to TCPP.

3.5. Photostability. High photostability is an important criterion for a fluorophore when applying it practically in biological systems. The effect of phosphonium cation on photostability of TCPP was investigated by performing a kinetic study. It has been proven that the addition of an IL-based counterion improves the photostability of macrocyclic dye molecules (e.g., porphyrins and phthalocyanines). Photostability of TCPP and [P₆₆₆₁₄]₄[TCPP] was determined over 1000 s after excitation at 420 nm and monitoring emission in kinetic mode at 650 nm with slit widths of

14-14 nm. Both compounds exhibit excellent stability in ethanol solvent (Figure S9 in the Supporting Information).

3.6. Fluorescence and phosphorescence lifetime. Fluorescence lifetimes of TCPP and [P₆₆₆₁₄]₄[TCPP] were measured in ethanol using TCSPC measurement. The decays were found to have a best fit of 2 exponentials. The lifetimes of both compounds are tabulated in Table 3. Most of the TCPP fluorescent species showed 9.5 ns lifetime while [P₆₆₆₁₄]₄[TCPP] chemo-PDT IM major component exhibited longer (10.5 ns) lifetime. These lifetimes are attributed to first excited singlet states (S₁). This longer lived S₁ state has a greater chance to undergo intersystem crossing to T₁ where reaction with molecular oxygen can occur.

Table 3 Fluorescence lifetimes of IM and parent TCPP in ethanol recorded at 390 nm excitation/650 nm emission.

Sample	τ_1 (ns)	α_1	τ_2 (ns)	α_2	χ^2
ТСРР	1.06	0.045	9.47	0.954	1.14
[P ₆₆₆₁₄] ₄ [TCPP]	0.57	0.043	10.52	0.957	1.23

Phosphorescence lifetime is a crucial factor in the effectiveness of a molecule to produce ROS. Decays for TCPP and [P₆₆₆₁₄]₄[TCPP] were measured in ethanol at 77 K and fitted using first exponential equation (Figure S10 in the Supporting Information). Decays were found to be 0.006 ms and 0.25 ms for TCPP and [P₆₆₆₁₄]₄[TCPP], respectively, in ethanol solvent. Conversion of porphyrin into IM exhibited a longer phosphorescence lifetime around two orders of magnitude. The longer triplet state lifetime of [P₆₆₆₁₄]₄[TCPP] allows more time to react with triplet oxygen molecules present in the cells before relaxing through phosphorescence. These lifetime results

demonstrate the possibility of a higher ROS quantum yield of the IM and thus should show a greater PDT effect than TCPP.

3.7. ROS/singlet oxygen quantum yield. The efficiency of a PDT drug is determined by calculating the ROS and singlet oxygen quantum yield values. Previously, both fluorescence and phosphorescence emission results indicated significant changes in the photophysical properties of the IM compared to TCPP. Thus, the generation of ROS in IMs are also likely to be affected. To investigate the efficiency of the PDT moiety in the combination drug, ROS quantum yield of parent TCPP and [P₆₆₆₁₄]₄[TCPP] IMs is determined using an ROS scavenging probe, DPBF. Photodegradation of DPBF upon reaction with radical oxygen species is well known and thus is a commonly used molecular probe for ROS detection. DPBF is insoluble in water, therefore quantum yield of INMs in aqueous media recorded later with ABDA probe. TCPP and [P₆₆₆₁₄]₄[TCPP] solutions in ethanol were prepared and used to investigate the ROS. DPBF is a radical scavenging molecule (yellow solution) that, upon selective reaction with ROS, is converted into 1,2-dibenzoylbenzene (colorless solution). Thus, the photo-degradation can easily be analyzed by monitoring the decrease in absorbance of DPBF at 411 nm using a spectrophotometer.

A solution of sample mixed with DPBF in ethanol was irradiated every 60 s for a total of 420 s at an excitation wavelength of 417 nm (Figure 3a). ROS quantum yield, Φ_{Δ} , was determined for each sample using Equation 4. ROS quantum yield for MB standard is 0.52 in ethanol solvent. The quantum yield value is doubled upon conversion of porphyrin into IM (Table 4). This is attributed to the presence of bulky phosphonium ions which inhibit porphyrin face-to-face aggregation that is detrimental to production of ROS.⁵⁵ It also verified that longer lived triplet state, improved phosphorescence emission intensity, and lower fluorescence quantum yield aided

to attain high singlet oxygen quantum yield for chemo-PDT combination drug based on IM as compared to parent compound.

In order to determine the singlet oxygen generation of INMs in aqueous solution, ABDA probe was used as a selective singlet oxygen scavenger. While ABDA is more selective towards singlet oxygen compared to other ROS, its sensitivity is much lower than DPBF. Thus, longer irradiation intervals of 150 s were used and absorbance was monitored at 380 nm. It was found that INMs generated singlet oxygen with a much faster rate as compared to MB or TCPP (Figure 3b). These results demonstrated that conversion of TCPP to IMs and INMs can greatly enhance their singlet oxygen quantum yield and thus their PDT efficiency. In order to confirm the decrease in absorbance of the probe is due to generation of singlet oxygen by the PS, a control experiment was designed where probe alone was irradiated. No significant decrease was observed for the probe, indicating that INMs are generating sufficient singlet oxygen under irradiation (Figure S11 in the Supporting Information).

Table 4. ROS/singlet oxygen quantum yield values obtained for each PS in ethanol or water solvent.

Solvent/Probe	MB	TCPP	[P ₆₆₆₁₄] ₄ [TCPP]
Ethanol/DPBF	0.52	0.14	0.28 (IM)
Water/ABDA	0.52	0.19	0.97 (INMs)

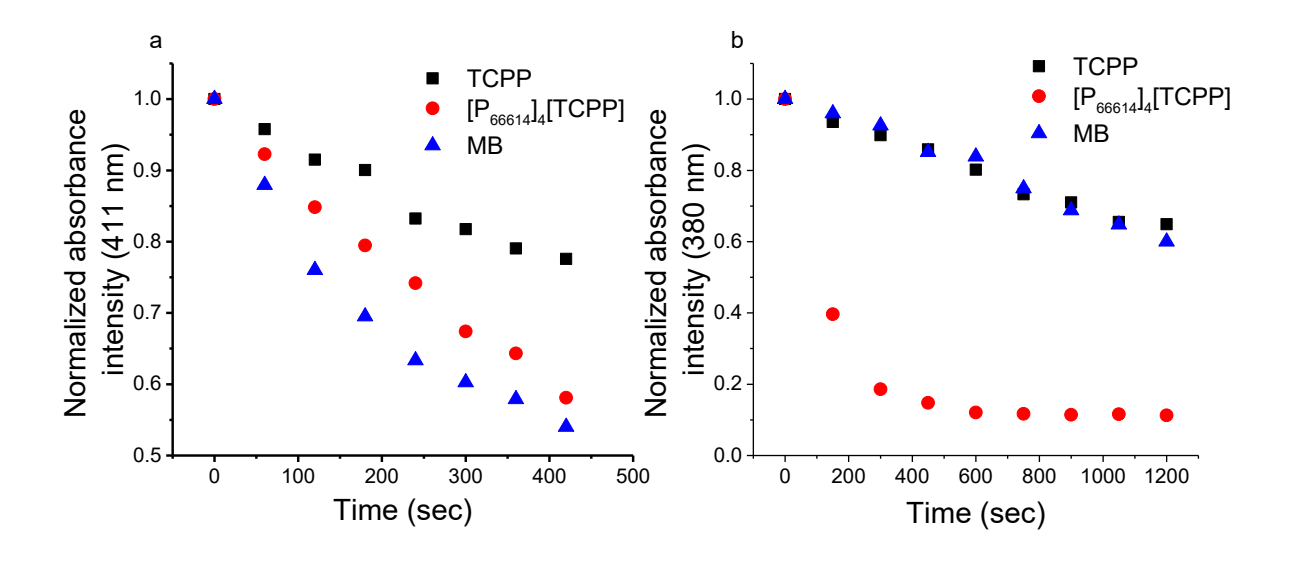


Figure 3. Photo-degradation of a) DPBF and b) ABDA upon increasing irradiation time in the presence of TCPP, $[P_{66614}]_4[TCPP]$ and MB. Final drug concentrations were 5 μ M and 10 μ M with DPBF and ABDA, respectively.

3.8. In vitro cellular toxicity of INMs and cellular uptake. After detailed characterization of newly developed combination IM and INMs, these materials were tested *in vitro* for their potential application as combination cancer therapy drugs. In this regard, human breast cancer cell line MCF-7 was selected and the half maximal inhibitory concentration (IC₅₀) of the drug was compared with its counterpart non-cancerous human breast cell line MCF-10A to determine the specificity of the drug towards cancerous cells. MTT assay was used to assess cell viability as a result of cytotoxic effects in the above mentioned cell lines incubated with [P₆₆₆₁₄]₄[TCPP] INMs, (P₆₆₆₁₄)Cl and TCPP parent molecule. All experiments were performed in 96 well plates with 10⁴ cells per well in triplicate to ensure replicable data. Statistical significance was determined by using a two-tailed student's t-test. To study concentration dependent cytotoxicity, cells were incubated with 0.5-20 μM of chemotherapeutic molecule and combination nanodrug for 24 hr followed by MTT assay.

The IC₅₀ value of the drug was analyzed by plotting the log of cell viability versus the concentration of drug and applying an exponential fit. It was shown that among both cell lines used, parent porphyrin molecule (TCPP) was not cytotoxic under the concentration range tested. For other drugs, the toxicity increased with an increase in concentration as expected. It is important to note that the combination drug contains four chemotherapeutic moieties per molecule, while the parent compound contains only one. However, the cytotoxicity of [P₆₆₆₁₄]₄[TCPP] in MCF-7 cell line is only about two times lower than the parent value (Table 5). This is attributed to the formation of stable NPs for the combination drug that have a different uptake mechanism compared to the parent molecule. Cell viability for each drug as a function of concentration in MCF-7 and MCF-10A cells is shown in Figure 4a and Figure S12 in the Supporting Information, respectively.

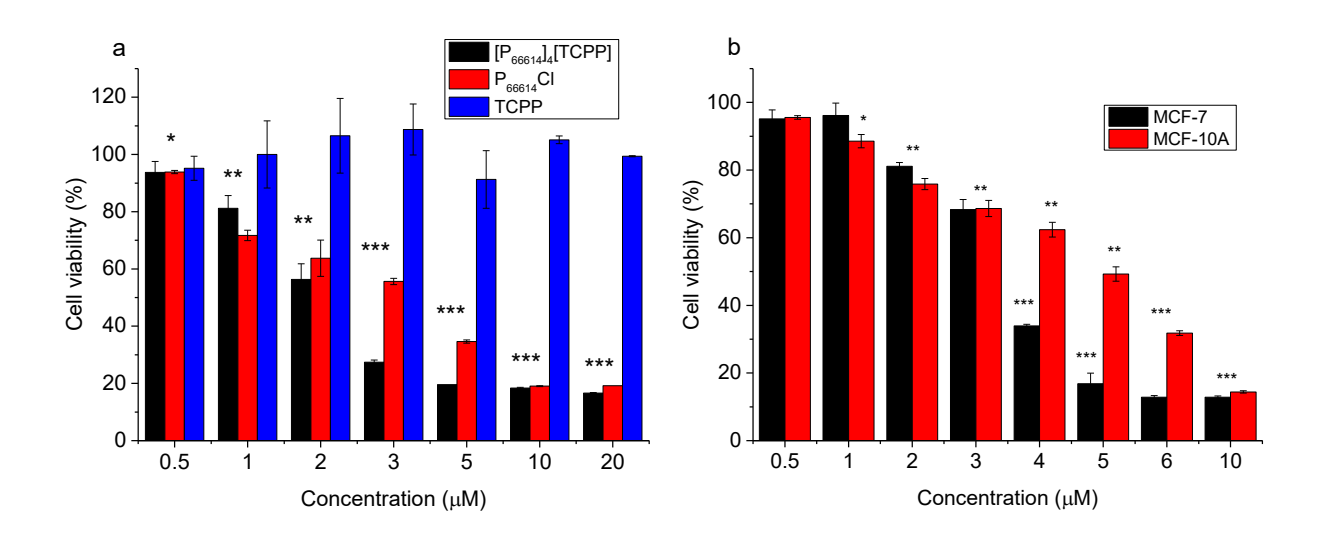


Figure 4. Cell viability of a) MCF-7 cells upon dosage with varying concentration of combination INMs and parent compounds (0.5-20 μ M) for 24 hr and b) FA-coated INMs incubated in cancer (MCF-7) and non-cancerous (MCF-10A) cell lines for 24 hr at concentration range of 0.5-10 μ M (* p<0.05, ** p<0.01, *** p<0.005).

The FA functionalized INMs, which is shown in literature to improve selectivity towards tumors, due to overexpression of FA receptors in many types of cancer cells, ^{36,57} can also aid in non-destructive and targeted delivery of NPs to cancer cells. ⁵⁸ FA functionalized INMs are labelled as FA-[P₆₆₆₁₄]₄[TCPP]. IC₅₀ value of FA-[P₆₆₆₁₄]₄[TCPP] in the cancer cell line was found to increase compared to non-FA coated INMs (Figure 4b), which could be due to the large solvated radius of FA-INMs that can affect passive uptake by EPR phenomenon less favorable. ⁵⁹ However, IC₅₀ of FA-coated INMs in non-cancerous cell line (MCF-10A) was greater than the same drug in MCF-7 cells (Table 5). The FA functionalized INMs showed selectivity towards cancer cells that wasn't observed for either drug without FA functionalization at the surface of NPs. This represents an easy and efficient approach to produce low-cost selective nanodrugs with combination mechanisms for cancer treatment.

Table 5. Calculated IC_{50} concentrations (μM) of drugs in different cell lines at 10^4 cells per well after 24 hr in dark

	IC ₅₀ concentration (μM)		
Cell line	P ₆₆₆₁₄ C1	[P ₆₆₆₁₄] ₄ [TCPP] INMs	FA-[P ₆₆₆₁₄] ₄ [TCPP] INMs
MCF-7	3.39±0.21	1.94±0.15	3.25±0.18
MCF-10A	3.28 ± 0.12	1.53±0.13	5.20±0.15

The dark *in vitro* studies validate the improved cyctotoxicity chemo-PDT INMs. Moreover, enabled selective toxicity towards cancerous cells was attained by functionalizing the INMs with FA. It should be noted that dark cytotoxicity results only account for the role of chemotheraputic ion in the combination INMs. Whereas, the counter anion of INMs can add its toxicity mechanism only upon light irrdation. In order to validate the dual mechanism (chemo-PDT) *in vitro*, light cytotoxicity experiments were performed. Briefly, TCPP or INMs were incubated in MCF-7 cells

for 4 hr, removed, and exposed to visible lamp light (0.14 W/cm², 10 min). For control, cells were left in the dark. Afterwards the cells were incubated an additional 24 hr and cell viability was determined by MTT assay. TCPP displays no dark toxicity under the concentration range used, however shows some toxicity under light irradiation (Figure 5a). [P₆₆₆₁₄]₄[TCPP] INMs show similar dark toxicity as previously determined with an increase in IC₅₀ due to decreased incubation time of 4 hr (Figure 5b). However, under light irradiation, INMs exhibit high light toxicity (Table S1 in the Supporting Information). The increased cytotoxicity of porphyrin in INMs in comparison to the parent compound is due to improved photophysical properties such as ROS and singlet oxygen qunatum yield. This study revealed that INMs approch can be utilized to attain enhanced PDT effect.

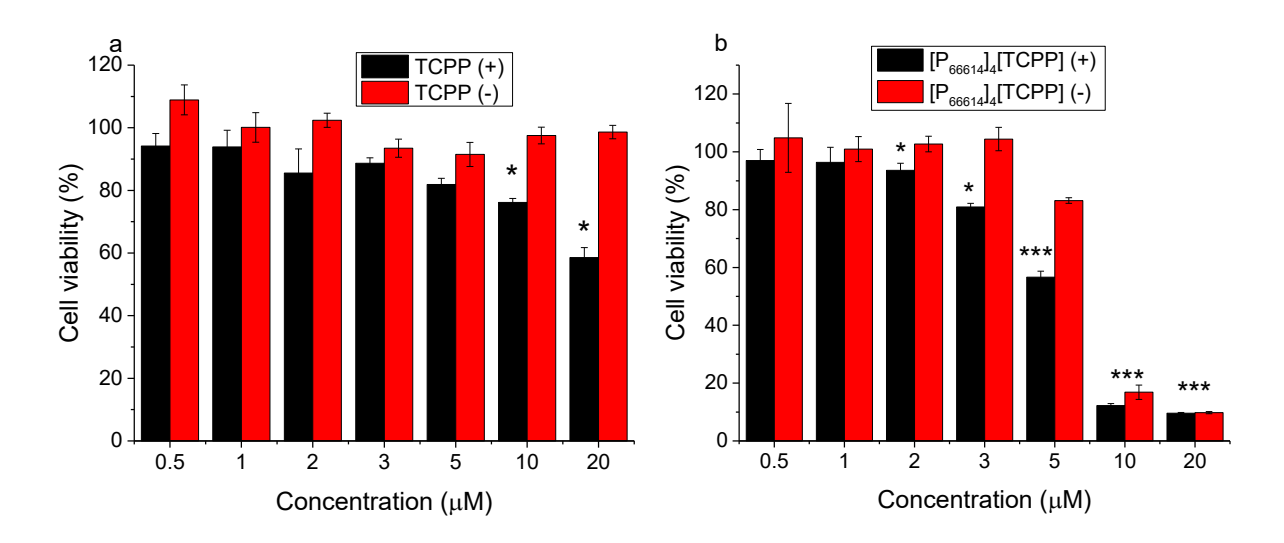


Figure 5. Toxicity of a) TCPP and b) $[P_{66614}]_4[TCPP]$ INMs after 4 hr incubation in MCF-7 cells under light irradiation, 0.14 W/cm² (+) or in dark (-) at a concentration range of 0.5-20 μ M (* p<0.05, ** p<0.01, *** p<0.005).

To further explain the mechanism of enhanced cytotoxicity of INMs, cellular uptake experiments were performed. Briefly, TCPP and INMs were separately incubated in a 6 well plate for 4 hr. Afterwards, the cells were washed thoroughly with PBS and dissolved with 100% DMSO solution. Spectrophotometer was used to determine the concentration of dissolved drug. It was

found that INMs were uptaken by cells 1.5 times more than TCPP after 4 hr (Figure 6). This shows that INMs exhibit enhanced cytotoxicity due to greater uptake by MCF-7 cells because of NP morphology, improved photophysical properties as well as dual mechanisms (chemotherapy along with PDT) present in a single nanodrug.

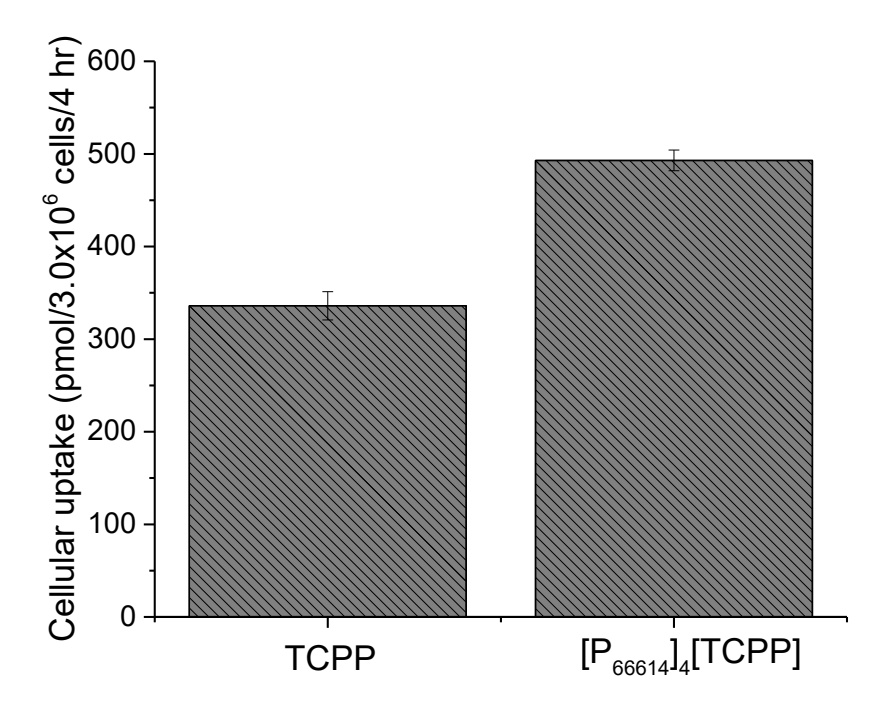


Figure 6. Cellular uptake of TCPP and INMs in MCF-7 cells after incubation of 4 nmol drug for 4 hr.

4. Conclusion

A facile one-step metathesis reaction was used to synthesize chemo-PDT combination IMs for the cancer therapy application for the first time. INMs are simply prepared using a reprecipitation method without adding any matrix. Conversion to IM reduced planar face aggregation of porphyrin units, thus shifting its wavelength maxima to a longer wavelength, which is important for deeper light penetration for PDT. The phosphorescence emission intensity of TCPP is enhanced upon conversion to IM along with the excited state lifetime which improved the PDT performance of

porphyrin anion in combination drug. The ROS quantum yield was doubled in value for IM

compared to TCPP which is expected due to long triplet state lifetime and reduced aggregation

compared to free porphyrin. Also, INMs displayed enhanced dark toxicity towards cancerous cells

due to enhanced cellular uptake of NPs based combination drug. Further, due to their superior

singlet oxygen production and light toxicity compared to TCPP, [P₆₆₆₁₄]₄[TCPP] INMs show great

potential as an all-in-one combination anticancer drug that is low-cost and simple to produce.

Furthermore, INMs' surface is functionalized with FA using simple ionic interactions, which aid

to tune the selectivity of the INMs towards cancer cells. The beauty in IL chemistry is the ease in

tunability as there are many different cytotoxic and photosensitizing combinations possible to

finely design a drug for the desired effects in vitro.

Supporting Information.

The following files are available free of charge.

Mass spectra, NMR, TEM imaging, DLS and zeta potential data, aggregation experiments, FA-

modified INMs photophysical characterization, phosphorescence spectra, photostability,

phosphorescence lifetime, absorbance of ABDA probe and IMs (control experiment) and MCF-

10A cytotoxicity are given in the Supporting Information document (PDF)

Corresponding Author

*Corresponding author: Noureen Siraj (E) nxsiraj@ualr.edu (O) 501-916-6544

Author Contributions

The manuscript was written through contributions of all authors. All authors have given approval

to the final version of the manuscript.

Author Information

28

Samantha Macchi: orcid.org/0000-0002-7546-4200

Mohd Zubair: orcid.org/0000-0002-4884-5200

Nawab Ali: orcid.org/0000-0002-0995-4965

Grégory Guisbiers: orcid.org/0000-0002-4615-6014

Noureen Siraj: orcid.org/0000-0003-4925-0265

Funding Sources

This publication was made possible by the Arkansas INBRE program, supported by a grant from

the National Institute of General Medical Sciences, (NIGMS), P20 GM103429 from the National

Institutes of Health. This material is based upon work supported in part by the National Science

Foundation EPSCoR Research Infrastructure under award number RII Track 4-1833004. Any

opinions, findings, and conclusions or recommendations expressed in this material are those of

the author(s) and do not necessarily reflect the views of the National Science Foundation.

Abbreviations

PDT, photodynamic therapy; FA, folic acid; TCPP, meso-tetra(4-carboxyphenyl)porphyrin;

INM, ionic nanomaterial; PS, photosensitizer; NP, nanoparticle; ABDA, 9,10-anthracenediyl-

bis(methylene)dimalonic acid; DPBF, 1,3-diphenylisobenzofuran; ROS, reactive oxygen species.

References

(1) Siegel, R. L.; Miller, K. D.; Jemal, A. Cancer Statistics, 2020. CA. Cancer J. Clin. 2020, 70

(1), 7–30. https://doi.org/10.3322/caac.21590.

(2) Hwang, H. S.; Shin, H.; Han, J.; Na, K. Combination of Photodynamic Therapy (PDT) and

Anti-Tumor Immunity in Cancer Therapy. J. Pharm. Investig. 2018, 48 (2), 143-151.

https://doi.org/10.1007/s40005-017-0377-x.

29

- (3) Wentrup, R.; Winkelmann, N.; Mitroshkin, A.; Prager, M.; Voderholzer, W.; Schachschal, G.; Jürgensen, C.; Büning, C. Photodynamic Therapy plus Chemotherapy Compared with Photodynamic Therapy Alone in Hilar Nonresectable Cholangiocarcinoma. *Gut Liver* 2016, 10 (3), 470–475. https://doi.org/10.5009/gnl15175.
- (4) Hou, W.; Zhao, X.; Qian, X.; Pan, F.; Zhang, C.; Yang, Y.; De La Fuente, J. M.; Cui, D. PH-Sensitive Self-Assembling Nanoparticles for Tumor near-Infrared Fluorescence Imaging and Chemo-Photodynamic Combination Therapy. *Nanoscale* **2016**, *8* (1), 104–116. https://doi.org/10.1039/c5nr06842h.
- (5) Ryan, Q.; Ibrahim, A.; Cohen, M. H.; Johnson, J.; Ko, C.; Sridhara, R.; Justice, R.; Pazdur, R. FDA Drug Approval Summary: Lapatinib in Combination with Capecitabine for Previously Treated Metastatic Breast Cancer That Overexpresses HER-2. *Oncologist* 2008, 13 (10), 1114–1119. https://doi.org/10.1634/theoncologist.2008-0816.
- (6) Blagosklonny, M. V. Analysis of FDA Approved Anticancer Drugs Reveals the Future of Cancer Therapy. *Cell Cycle* **2004**, *3* (8), 1035–1042. https://doi.org/10.4161/cc.3.8.1023.
- (7) Cheng, Z.; Al Zaki, A.; Hui, J. Z.; Muzykantov, V. R.; Tsourkas, A. Multifunctional Nanoparticles: Cost versus Benefit of Adding Targeting and Imaging Capabilities. *Science* (80-.). **2012**, 338 (6109), 903–910. https://doi.org/10.1126/science.1226338.
- (8) Zhou, J.; Lu, Z.; Zhu, X.; Wang, X.; Liao, Y.; Ma, Z.; Li, F. NIR Photothermal Therapy Using Polyaniline Nanoparticles. *Biomaterials* 2013, 34 (37), 9584–9592. https://doi.org/10.1016/j.biomaterials.2013.08.075.
- (9) Lee, J. H.; Nan, A. Combination Drug Delivery Approaches in Metastatic Breast Cancer. *J. Drug Deliv.* **2012**, *2012*, 1–17. https://doi.org/10.1155/2012/915375.
- (10) Warner, I. M.; El-Zahab, B.; Siraj, N. Perspectives on Moving Ionic Liquid Chemistry into the Solid Phase. *Anal. Chem.* **2014**, *86* (15), 7184–7191. https://doi.org/10.1021/ac501529m.
- (11) Siraj, N.; Hasan, F.; Das, S.; Kiruri, L. W.; Steege Gall, K. E.; Baker, G. A.; Warner, I. M. Carbazole-Derived Group of Uniform Materials Based on Organic Salts: Solid State

- Fluorescent Analogues of Ionic Liquids for Potential Applications in Organic-Based Blue Light-Emitting Diodes. **2014**, *118* (5), 2312–2320. https://doi.org/10.1021/jp410784v.
- (12) Siraj, N.; Das, S.; Hasan, F.; Lu, C.; Kiruri, L. W.; Steege Gall, K. E.; Warner, I. M. Enhanced S2 Emission in Carbazole-Based Ionic Liquids. *RSC Adv.* **2015**, *5* (13), 9939–9945. https://doi.org/10.1039/c4ra12362j.
- (13) Siraj, N.; Magut, P. K. S.; Mcdonough, K.; Sahasrabudhe, G.; Warner, I. M. Endocytic Selective Toxicity of Rhodamine 6G NanoGUMBOS in Breast Cancer Cells. 2018, 15 (9), 3837–3845. https://doi.org/10.1021/acs.molpharmaceut.8b00339.
- (14) Kolic, P. E.; Siraj, N.; Cong, M.; Regmi, B. P.; Luan, X.; Wang, Y.; Warner, I. M. Improving Energy Relay Dyes for Dye-Sensitized Solar Cells by Use of a Group of Uniform Materials Based on Organic Salts (GUMBOS). RSC Adv. 2016, 6 (97), 95273–95282. https://doi.org/10.1039/c6ra21980b.
- (15) Macchi, S.; Zubair, M.; Ali, N.; Guisbiers, G.; Siraj, N. Tunable Cytotoxicity and Selectivity of Phosphonium Ionic Liquid with Aniline Blue Dye. *J. Nanosci. Nanotechnol.* 2021, 21 (12), 6143–6150. https://doi.org/10.1166/JNN.2021.19535.
- (16) Le, T.; Macchi, S.; Jalihal, A.; Szwedo, S.; Siraj, N. Paper-Based Portable Sensor and Nanosensor For Sulfur Dioxide Detection. *Curr. Res. Mater. Chem.* **2021**, *3* (1), 109.
- Berton, P.; Siraj, N.; Das, S.; Rooy, S. de; Wuilloud, R. G.; Warner, I. M. Efficient Low-(17)Cost Procedure for Microextraction of Estrogen from Environmental Water Using Magnetic Mol. 2021. Vol. 26. Page 32 2020, 26 Ionic Liquids. (1),32. https://doi.org/10.3390/MOLECULES26010032.
- (18) Kumar, V.; Malhotra, S. V. Antitumor Activity of Ionic Liquids on Human Tumor Cell Lines. In *ACS Symposium Series*; UTC, 2010; Vol. 1038, pp 91–102. https://doi.org/10.1021/bk-2010-1038.ch008.
- (19) Kumar, V.; Malhotra, S. V. Bioorganic & Medicinal Chemistry Letters Study on the Potential Anti-Cancer Activity of Phosphonium and Ammonium-Based Ionic Liquids. *Bioorg. Med. Chem. Lett.* 2009, 19 (16), 4643–4646.

- https://doi.org/10.1016/j.bmcl.2009.06.086.
- (20) Moodley, K. G. Roles of Ionic Liquids in Medicines for the Treatment of Cancer and Tuberculosis. *Der Pharma Chem.* **2019**, *11* (1), 1–19.
- (21) Hough, W. L.; Smiglak, M.; Rodríguez, H.; Swatloski, R. P.; Spear, S. K.; Daly, D. T.; Pernak, J.; Grisel, J. E.; Carliss, R. D.; Soutullo, M. D.; Davis, J. H.; Rogers, R. D. The Third Evolution of Ionic Liquids: Active Pharmaceutical Ingredients. *New J. Chem.* **2007**, *31* (8), 1429–1436. https://doi.org/10.1039/b706677p.
- (22) Master, A.; Livingston, M.; Sen Gupta, A. Photodynamic Nanomedicine in the Treatment of Solid Tumors: Perspectives and Challenges. *J. Control. Release* **2013**, *168* (1), 88–102. https://doi.org/10.1016/j.jconrel.2013.02.020.
- (23) Kruger, C. A.; Abrahamse, H. Utilisation of Targeted Nanoparticle Photosensitiser Drug Delivery Systems for the Enhancement of Photodynamic Therapy. *Molecules* **2018**, *23* (10). https://doi.org/10.3390/molecules23102628.
- (24) Hu, C.-M. J.; Aryal, S.; Zhang, L. Nanoparticle-Assisted Combination Therapies for Effective Cancer Treatment. *Ther. Deliv.* **2010**, *1* (2), 323–334. https://doi.org/10.4155/tde.10.13.
- (25) Bae, K. H.; Chung, H. J.; Park, T. G. Nanomaterials for Cancer Therapy and Imaging. *Mol. Cells* **2011**, *31* (4), 295–302. https://doi.org/10.1007/s10059-011-0051-5.
- (26) Onoue, S.; Yamada, S.; Chan, H. K. Nanodrugs: Pharmacokinetics and Safety. *Int. J. Nanomedicine* **2014**, *9* (1), 1025–1037. https://doi.org/10.2147/IJN.S38378.
- (27) Zhang, R.; Xing, R.; Jiao, T.; Chen, C.; Ma, K.; Ma, G.; Yan, X. Carrier-Free, Chemophotodynamic Dual Nanodrugs via Self-Assembly for Synergistic Antitumor Therapy. *ACS Appl. Mater. Interfaces* **2016**, *8* (21), 13262–13269.
- (28) Cuenca, A. G.; Jiang, H.; Hochwald, S. N.; Delano, M.; Cance, W. G.; Grobmyer, S. R. Emerging Implications of Nanotechnology on Cancer Diagnostics and Therapeutics. *Cancer* **2006**, *107* (3), 459–466. https://doi.org/10.1002/cncr.22035.

- (29) Diaz-Uribe, C. E.; Daza, M. C.; Páez-Mozo, E. A.; Martínez O., F.; Guedes, C. L. B.; Di Mauro, E. Visible Light Singlet Oxygen Production with Tetra(4-Carboxyphenyl) Porphyrin/SiO2. J. Photochem. Photobiol. A Chem. 2013, 259, 47–52. https://doi.org/10.1016/j.jphotochem.2013.03.005.
- (30) Debele, T. A.; Peng, S.; Tsai, H. C. Drug Carrier for Photodynamic Cancer Therapy. *Int. J. Mol. Sci.* **2015**, *16* (9), 22094–22136. https://doi.org/10.3390/ijms160922094.
- (31) Miao, W.; Kim, H.; Gujrati, V.; Kim, J. Y.; Jon, H.; Lee, Y.; Choi, M.; Kim, J.; Lee, S.; Lee, D. Y.; Kang, S.; Jon, S. Photo-Decomposable Organic Nanoparticles for Combined Tumor Optical Imaging and Multiple Phototherapies. *Theranostics* 2016, 6 (13), 2367–2379. https://doi.org/10.7150/thno.15829.
- (32) Sun, X.; Zebibula, A.; Dong, X.; Li, G.; Zhang, G.; Zhang, D.; Qian, J.; He, S. Targeted and Imaging-Guided in Vivo Photodynamic Therapy for Tumors Using Dual-Function, Aggregation-Induced Emission Nanoparticles. *Nano Res.* 2018, 11 (5), 2756–2770. https://doi.org/10.1007/s12274-017-1906-7.
- (33) Rui, L. L.; Cao, H. L.; Xue, Y. D.; Liu, L. C.; Xu, L.; Gao, Y.; Zhang, W. A. Functional Organic Nanoparticles for Photodynamic Therapy. *Chinese Chem. Lett.* **2016**, *27* (8), 1412–1420. https://doi.org/10.1016/j.cclet.2016.07.011.
- (34) Hong, E. J.; Choi, D. G.; Shim, M. S. Targeted and Effective Photodynamic Therapy for Cancer Using Functionalized Nanomaterials. *Acta Pharm. Sin. B* **2016**, *6* (4), 297–307. https://doi.org/10.1016/j.apsb.2016.01.007.
- (35) Van Vlerken, L. E.; Vyas, T. K.; Amiji, M. M. Poly(Ethylene Glycol)-Modified Nanocarriers for Tumor-Targeted and Intracellular Delivery. *Pharm. Res.* **2007**, *24* (8), 1405–1414. https://doi.org/10.1007/s11095-007-9284-6.
- (36) Chen, C.; Ke, J.; Edward Zhou, X.; Yi, W.; Brunzelle, J. S.; Li, J.; Yong, E. L.; Xu, H. E.; Melcher, K. Structural Basis for Molecular Recognition of Folic Acid by Folate Receptors. *Nature* **2013**, *500* (7463), 486–489. https://doi.org/10.1038/nature12327.
- (37) Cheung, A.; Bax, H. J.; Josephs, D. H.; Ilieva, K. M.; Pellizzari, G.; Opzoomer, J.;

- Bloomfield, J.; Fittall, M.; Grigoriadis, A.; Figini, M.; Canevari, S.; Spicer, J. F.; Tutt, A. N.; Karagiannis, S. N. Targeting Folate Receptor Alpha for Cancer Treatment. *Oncotarget* **2016**, *7* (32), 52553–52574. https://doi.org/10.18632/oncotarget.9651.
- (38) Lin, Y.; Zhou, T.; Bai, R.; Xie, Y. Chemical Approaches for the Enhancement of Porphyrin Skeleton-Based Photodynamic Therapy. *J. Enzyme Inhib. Med. Chem.* **2020**, *35* (1), 1080–1099. https://doi.org/10.1080/14756366.2020.1755669.
- (39) Liu, S.; Hu, Y.; Hu, C.; Xiong, Y.; Duan, M. Quantum Yields of Singlet Oxygen of Tetrakis (4-Carboxyphenyl) Porphyrin in Different Solvents. *J. Porphyr. Phthalocyanines* **2019**, 1–8. https://doi.org/10.1142/S1088424619501207.
- (40) Mosinger, J.; Deumié, M.; Lang, K.; Kubát, P.; Wagnerová, D. M. Supramolecular Sensitizer: Complexation of Meso-Tetrakis(4-Sulfonatophenyl)Porphyrin with 2-Hydroxypropyl-Cyclodextrins. *J. Photochem. Photobiol. A Chem.* **2000**, *130* (1), 13–20. https://doi.org/10.1016/S1010-6030(99)00204-X.
- (41) Kolic, P. E.; Siraj, N.; Hamdan, S.; Regmi, B. P.; Warner, I. M. Synthesis and Characterization of Porphyrin-Based GUMBOS and NanoGUMBOS as Improved Photosensitizers. *J. Phys. Chem. C* **2016**, *120* (9), 5155–5163. https://doi.org/10.1021/acs.jpcc.5b12013.
- (42) Siraj, N.; Kolic, P. E.; Regmi, B. P.; Warner, I. M. Strategy for Tuning the Photophysical Properties of Photosensitizers for Use in Photodynamic Therapy. *Chem. A Eur. J.* **2015**, 21 (41), 14440–14446. https://doi.org/10.1002/chem.201501686.
- (43) Li, M.; Yu, C.; Hu, C.; Yang, W.; Zhao, C.; Wang, S.; Zhang, M.; Zhao, J.; Wang, X.; Qiu, J. Solvothermal Conversion of Coal into Nitrogen-Doped Carbon Dots with Singlet Oxygen Generation and High Quantum Yield. *Chem. Eng. J.* **2017**, *320*, 570–575. https://doi.org/10.1016/J.CEJ.2017.03.090.
- (44) Kilaparty, S. P.; Agarwal, R.; Singh, P.; Kannan, K.; Ali, N. Endoplasmic Reticulum Stress-Induced Apoptosis Accompanies Enhanced Expression of Multiple Inositol Polyphosphate Phosphatase 1 (Minpp1): A Possible Role for Minpp1 in Cellular Stress Response. *Cell*

- Stress Chaperones **2016**, 21 (4), 593–608. https://doi.org/10.1007/s12192-016-0684-6.
- (45) Lambert, C. R.; Reddi, E.; Spikes, J. D.; Rodgers, M. A. J.; Jori, G. The Effects of Porphyrin Structure and Aggregation State on Photosensitized Processes in Aqueous and Micellar Media. *Photochem. Photobiol.* **1986**, *44* (5), 595–601. https://doi.org/10.1111/j.1751-1097.1986.tb04714.x.
- (46) Kano, K.; Fukuda, K.; Wakami, H.; Nishiyabu, R.; Pasternack, R. F. Factors Influencing Self-Aggregation Tendencies of Cationic Porphyrins in Aqueous Solution. *J. Am. Chem. Soc.* **2000**, *122* (31), 7494–7502. https://doi.org/10.1021/JA000738G.
- (47) Friesen, B. An Investigation of Porphyrin Aggregation Using Spectroscopic and Microscopic Methods, 2011, 1.
- (48) Pasternack, R. F.; Fleming, C.; Herring, S.; Collings, P. J.; DePaula, J.; DeCastro, G.; Gibbs, E. J. Aggregation Kinetics of Extended Porphyrin and Cyanine Dye Assemblies. *Biophys. J.* **2000**, *79* (1), 550–560. https://doi.org/10.1016/S0006-3495(00)76316-8.
- (49) Zhang, D. W.; Chen, W. T. Two Novel Tcpp Porphyrinic Compounds: In Situ Syntheses, Characterization and Reaction Mechanism. *J. Chil. Chem. Soc.* 2017, 62 (1), 3381–3385. https://doi.org/10.4067/S0717-97072017000100015.
- (50) Hoche, J.; Schulz, A.; Dietrich, L. M.; Humeniuk, A.; Stolte, M.; Schmidt, D.; Brixner, T.; Würthner, F.; Mitric, R. The Origin of the Solvent Dependence of Fluorescence Quantum Yields in Dipolar Merocyanine Dyes. *Chem. Sci.* 2019, 10 (48), 11013–11022. https://doi.org/10.1039/c9sc05012d.
- (51) Ho-Wu, R.; Yau, S. H.; Goodson, T. Efficient Singlet Oxygen Generation in Metal Nanoclusters for Two-Photon Photodynamic Therapy Applications. *J. Phys. Chem. B* **2017**, *121* (43), 10073–10080. https://doi.org/10.1021/acs.jpcb.7b09442.
- (52) Marin, D. M.; Payerpaj, S.; Collier, G. S.; Ortiz, A. L.; Singh, G.; Jones, M.; Walter, M. G. Efficient Intersystem Crossing Using Singly Halogenated Carbomethoxyphenyl Porphyrins Measured Using Delayed Fluorescence, Chemical Quenching, and Singlet Oxygen Emission. *Phys. Chem. Chem. Phys.* 2015, 17 (43), 29090–29096.

- https://doi.org/10.1039/c5cp04359j.
- (53) Spiller, W.; Kliesch, H.; Wöhrle, D.; Hackbarth, S.; Röder, B.; Schnurpfeil, G. Singlet Oxygen Quantum Yields of Different Photo-Sensitizers in Polar Solvents and Micellar Solutions. *J. Porphyr. Phthalocyanines* **1998**, *2* (2), 145–158. https://doi.org/https://doi.org/10.1002/(SICI)1099-1409(199803/04)2:2<145::AID-JPP60>3.0.CO;2-2.
- (54) Schmitz, C.; Aubry, J. M.; Rigaudy, J. A New Access to the Anthracene Core. Synthesis of Two Water Soluble Singlet Oxygen Traps Derived from 1,3-Diphenylisobenzofuran and 9,10-Diphenylanthracene. *Tetrahedron* **1982**, *38* (10), 1425–1430. https://doi.org/10.1016/0040-4020(82)80224-X.
- (55) Tanielian, C.; Schweitzer, C.; Mechin, R.; Wolff, C. Quantum Yield of Singlet Oxygen Production by Monomeric and Aggregated Forms of Hematoporphyrin Derivative. *Free Radic. Biol. Med.* **2001**, *30* (2), 208–212. https://doi.org/10.1016/S0891-5849(00)00460-3.
- (56) Entradas, T.; Waldron, S.; Volk, M. The Detection Sensitivity of Commonly Used Singlet Oxygen Probes in Aqueous Environments. *J. Photochem. Photobiol. B Biol.* **2020**, *204*, 111787. https://doi.org/10.1016/j.jphotobiol.2020.111787.
- (57) Kelemen, L. E. The Role of Folate Receptor α in Cancer Development, Progression and Treatment: Cause, Consequence or Innocent Bystander? *Int. J. Cancer* **2006**, *119* (2), 243–250. https://doi.org/10.1002/ijc.21712.
- (58) Leamon, C. P.; Low, P. S. Delivery of Macromolecules into Living Cells: A Method That Exploits Folate Receptor Endocytosis. *Proc. Natl. Acad. Sci. U. S. A.* **1991**, *88* (13), 5572–5576. https://doi.org/10.1073/pnas.88.13.5572.
- (59) Gao, J. Q.; Eto, Y.; Yoshioka, Y.; Sekiguchi, F.; Kurachi, S.; Morishige, T.; Yao, X.; Watanabe, H.; Asavatanabodee, R.; Sakurai, F.; Mizuguchi, H.; Okada, Y.; Mukai, Y.; Tsutsumi, Y.; Mayumi, T.; Okada, N.; Nakagawa, S. Effective Tumor Targeted Gene Transfer Using PEGylated Adenovirus Vector via Systemic Administration. *J. Control. Release* 2007, 122 (1), 102–110. https://doi.org/10.1016/j.jconrel.2007.06.010.

TOC Graphic

